Lattice curvature induced substrate X-ray line broadening in InGaP/GaAs heterostructures

J. W. Lee, M. S. Oh, J. Y. Kim and T. I. Kim

Samsung Advanced Institute of Technology, LD Project Lab., P.O. Box 111, Suwon 440-600 (South Korea)

(Received December 31, 1994; in revised form April 19, 1994)

Abstract

The interfacial coherency of InGaP/GaAs heterostructure wafers grown by the metal-organic chemical vapor deposition technique is examined and its effects on the X-ray line broadening of the GaAs substrate are investigated. Lattice mismatches are measured using both (400) symmetric and {511} asymmetric reflections. The strain-free chemical lattice misfit and the elastic strain are also calculated. The X-ray full width at half maximum (FWHM) of the substrate is measured, and its dependence on the degree of lattice mismatch is found. In order to understand this observation, measurements of lattice curvature are carried out using the automatic Bragg angle control method. It is found that the radius of curvature varies with the elastic strain and the substrate FWHM. Using the results obtained, the misfit stress is also determined. Various contributions to the substrate line broadening are separated out. Calculated line widths are shown to be in good agreement with measured values. It is thus concluded that the primary factor affecting the X-ray line width of the substrate is misfit stress induced lattice curvature. The results presented demonstrate that interfacial coherency is of major importance in influencing the structural properties of InGaP/GaAs heterostructures through elastic strain and lattice curvature.

1. Introduction

InGaP/GaAs heterostructures have attracted extensive interest because they can be used for fabrication of visible laser diodes [1,2] and high speed devices [3]. One of the major requirements in the fabrication of perfect heterostructures is minimization of the misfit stress and strain which are caused by lattice mismatch between the epilayer and the substrate. Large lattice mismatch is readily introduced particularly in the InGaP/GaAs system due to large differences in lattice parameters among InP, GaP and GaAs. Misfit stress of the heterostructures has been shown to be one of the factors influencing wafer properties such as lattice curvature and device reliability [4,5]. Thus, precise determination of stress is needed to improve material quality and device performance.

It is well known [6–8] that double crystal X-ray diffractometry (DXRD) is a powerful and sensitive technique for evaluating the elastic response of materials. DXRD profiles provide a wealth of information on the structural properties of the crystal. For example, lattice mismatch between the epilayer and the substrate, line width, and elastic curvature can be

determined by DXRD. Among these features, the shape and line width of the epilayer peak obtained from the DXRD profile have been investigated extensively [7,9–11] because they can be used as an indirect measure of epilayer quality. However, the X-ray line broadening of the substrate has not attracted as much attention, in spite of the fact that it also provides some important structural features including misfit stress and lattice curvature. It is thus important to systematically calculate the stress acting on the wafer, and to determine the contribution from misfit stress to total substrate line broadening.

A series of $\ln_x Ga_{1-x}P$ epilayers with a relatively large range of lattice mismatches have been grown on (100) GaAs substrate by metal-organic chemical vapor deposition (MOCVD) and have been examined by DXRD. In this study, the influence of lattice coherency and misfit stress on the X-ray line broadening of the GaAs substrate is investigated. Firstly, various interfacial parameters such as lattice mismatch and elastic strain are determined. Secondly, dependence of the substrate line width and lattice curvature on the lattice coherency is discussed. Also, misfit stress caused by lattice misfit is calculated. Finally, based on the results

obtained, the dominant factor for substrate line broadening is determined.

2. Experimental details

InGaP/GaAs single heterostructure wafers grown by MOCVD were examined in this study. They consist of two layers: an undoped InGaP epilayer ($\sim 1 \mu m$) and a *n*-GaAs buffer layer ($\sim 0.2 \mu \text{m}$, $n(\text{Si}) \sim 1 \times 10^{18} \text{ cm}^{-3}$) on a (100) GaAs substrate ($\sim 350 \mu m$). The reactants for MOCVD growth were triethylgallium, trimethylindium, and phosphine at a temperature of 640 °C. The layer thickness was determined by direct measurement on a scanning electron microscope. Alloy composition was varied such that the lattice mismatch ranged from about -1.9×10^{-3} to 1.2×10^{-3} . The composition of each sample was determined by the peak separation in the DXRD profile. Indium content ranged from 45.8 to 50.1 for the samples used in this investigation. Measurements of interfacial coherency performed using a Bede DXRD (model 200) using Cu $K\alpha_1$ radiation ($\lambda = 0.154056$ nm). The (220) reflection from the Si first crystal was used to provide a highly parallel incident beam. The X-ray beam was conditioned using a channel cut collimator. (400) and {511} reflections were employed to calculate both normal and parallel mismatches. The presence of misfit dislocations was examined by X-ray double crystal topography.

3. Results and discussion

3.1. Lattice coherency measurement

In order to investigate the lattice coherency between the InGaP epilayer and the GaAs substrate, mismatch measurements were extensively performed for all the specimens used in this study. The normal mismatch $\Delta a_{\rm q}^{\perp}/a_{\rm b}$ (where $\Delta a_{\rm q}^{\perp}=a_{\rm q}^{\perp}-a_{\rm b}$) and the parallel mismatch $\Delta a_{\rm q}^{\parallel}/a_{\rm b}$ (where $\Delta a_{\rm q}^{\parallel}=a_{\rm q}^{\parallel}-a_{\rm b}$) were calculated using both (400) symmetric and {511} asymmetric reflections. The quantities, $a_{\rm q}^{\perp}$ and $a_{\rm q}^{\parallel}$, are the lattice parameters of the InGaP epilayer normal and parallel to the wafer surface, respectively, and $a_{\rm b}$ is the lattice constant of the GaAs substrate.

The angular separation, $\Delta\theta$, between the epilayer and the substrate peak in the (400) reflection is caused by tetragonal distortion of the InGaP epilayer normal to the wafer surface. The normal mismatch in the (400) symmetric reflection was calculated by noting the difference in peak positions of the substrate and the epilayer. This is calculated by [12]

$$\Delta a_{\rm g}^{\perp}/a_{\rm b} = -\Delta \theta/\tan \theta_{\rm B} \tag{1}$$

where θ_B is the Bragg angle of the (400) reflection and $\Delta\theta$ is the angular separation in (400).

As mentioned elsewhere [13,14], $\Delta\theta_1$ and $\Delta\theta_2$ in (511) and (-511) setting can be obtained by rotating the specimen by 180° around the axis parallel to [511] direction such that the incoming X-ray beam in one setting becomes the outgoing beam in the other setting. The quantities, $\Delta\theta$ and $\Delta\pi$ in the {511} reflection are due to different d-spacing and different tilt angle of reflecting planes in the epilayer and the substrate, respectively. These can be calculated by

$$\Delta \theta = (\Delta \theta_1 + \Delta \theta_2)/2$$

$$\Delta \pi = (\Delta \theta_1 - \Delta \theta_2)/2$$
(2)

Using the experimentally obtained quantities, the normal and the parallel mismatches were calculated as shown in Table 1. The normal and the parallel mismatches in the {511} setting were calculated by

$$\Delta a_{\mathbf{q}}^{\perp}/a_{\mathbf{b}} = -(\tan \pi \ \Delta \pi + \cot \theta \ \Delta \theta)$$

$$\Delta a_{\mathbf{q}}^{\parallel}/a_{\mathbf{b}} = \cot \pi \ \Delta \pi - \cot \theta \ \Delta \theta$$
(3)

where θ is the Bragg angle for the $\{511\}$ reflection and π is the angle between the $\{511\}$ planes and the wafer surface. It should be noted from the results in Table 1 that the normal mismatches determined by the (400) and $\{511\}$ reflections are virtually identical, indicating the internal consistency of the two reflections. It is also found that the normal mismatches are more than 25 times larger than the parallel mismatches. This illustrates that, for all the samples used in this study, the composition induced lattice misfit is accommodated almost entirely by elastic strain (tetragonal distortion) and that the heterointerface between the epilayer and the substrate is coherent.

In order to experimentally verify the existence of dislocations in the samples, X-ray double crystal reflection topography was performed for all the specimens using the (400) reflection [15–17]. Fig. 1 shows, for

Table 1 Normal and parallel mismatches determined from (400) and $\{511\}$ reflections

Sample	(400) Normal $(\times 10^{-3})$	$\{511\}$ Normal $(\times 10^{-3})$	$\{511\}$ Parallel $(\times 10^{-3})$
1	2.43	2.34	> 0.1
2	1.82	1.75	> 0.1
3	0.97	0.95	> 0.1
4	0.95	0.94	> 0.1
5	-0.61	-0.67	> -0.1
6	-1.64	-1.57	> -0.1
7	-1.68	-1.76	> -0.1
8	-1.89	-1.93	> -0.1
9	-3.14	-3.72	> -0.2

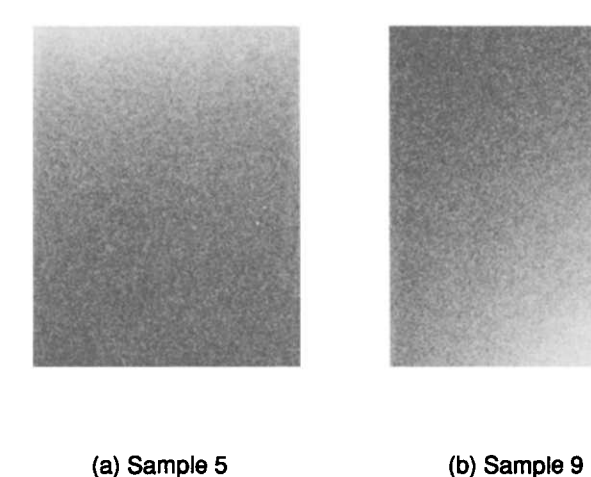


Fig. 1. Double crystal reflection X-ray topographs taken at the Bragg angle of the InGaP epilayer. (a) Sample 5; (b) sample 9. In both figures, the sample dimension traversed is 0.7 mm.

example, two double crystal reflection X-ray topographs obtained from sample 5 (Fig. 1(a)) and sample 9 (Fig. 1(b)). Note that these two samples have the smallest and the largest lattice mismatches among the samples used in this study. It can be seen that no structural defects are present in both samples, indicating that dislocations are absent. Provided that dislocations were present in the specimen, these would give rise to reflecting power differences, which in turn lead to contrasting differences in the photographic image. Thus, dislocations would have been readily imaged, if present, using this topographic method. In the topographic images in Fig. 1, a uniform greyness is observed. There are two different ways to interpret this observation: (a) there are no dislocations present; (b) there are dislocations whose density exceeds the upper limit for resolvable observation of individual dislocations. Note that the latter includes the possibility that although the dislocations may be present, the X-ray penetration depth is insufficient to reach the strain field of the dislocations.

A calculation was made to estimate the X-ray penetration depth into the sample using the following equation [18]:

$$\frac{I}{I_0} = \exp\left(\sum_{i=1}^n -\mu_i \alpha t_i\right) \tag{4}$$

where I/I_0 is the ratio of the diffracted and incident beam, μ_i is the mass absorption coefficient of the *i*th layer, n is the number of layers, α is a geometrical constant, and t_i is the thickness of each layer. The structure is 1.5 μ m thick and the absorption depth calculated from the linear absorption coefficients is larger than 10 μ m, so it is expected that reflections from all layers and the substrate will be detected when using Cu K α_1 radiation with the (400) reflection. According to this calculation, the penetration depth into the specimen is large enough that the dislocated region is reached. The possibility of case (b) mentioned above is thus eliminated. Therefore, the dislocations are absent in our samples in the range of mismatch values under this investigation. This is in good agreement with another result [19] that the transition from elastic to plastic deformation occurs at the lattice misfit value of $\sim 2.5 \times 10^{-3}$. Note that the largest lattice misfit value in our samples is $\sim 1.8 \times 10^{-3}$, as seen in Table 2. It is thus expected that the lattice misfit in all the specimens should be accommodated elastically in the range of lattice misfit values in this study.

For further investigation of lattice coherency, the strain-free lattice parameter of the epilayer, the lattice misfit, and the elastic strain were calculated as shown in Table 2. Once the lattice mismatches are determined by symmetric and asymmetric reflections, it is relatively simple to calculate the lattice misfit induced by compositional change alone. The lattice mismatch between the epilayer and the substrate in the absence of epitaxy is called lattice misfit hereafter. When the parallel mismatch is nearly equal to 0 as shown in Table 1, the lattice misfit $(\Delta a/a)_0$ can be defined by [20]

$$\left(\frac{\Delta a}{a}\right)_0 = \frac{1 - \nu}{1 + \nu} \left(\frac{\Delta a_{\rm q}^{\perp}}{a_{\rm b}}\right) \tag{5}$$

where ν is Poisson's ratio (assumed to be 1/3).

The strain-free lattice parameter of the epilayer can be directly determined from the lattice misfit. For this calculation, the lattice misfit is redefined by

$$(\Delta a/a)_0 = (a_0^{\text{s.f.}} - a_b)/a_b \tag{6}$$

where $a_q^{\text{s.f.}}$ is the strain-free lattice parameter of the InGaP epilayer in the absence of epitaxy. The lattice parameter of the GaAs substrate is assumed to be 0.56532 nm [21].

Whereas the lattice misfit is defined in relation to the substrate, the elastic strain ε is defined by the parallel strain of the epilayer alone:

$$\varepsilon = (a_{\mathbf{q}}^{\parallel} - a_{\mathbf{q}}^{\text{s.f.}})/a_{\mathbf{q}}^{\text{s.f.}} \tag{7}$$

Note from Table 2 that the elastic strain increases along with the lattice misfit as the value of the lattice mismatch changes. This indicates that the elastic strain is proportional to the magnitude of the lattice misfit within an elastic limit.

The anisotropy of strain and relaxation has been reported recently [22,23]. In order to examine the possible presence of this phenomena in our samples, the parallel mismatches and strains were measured not only along the [110] direction (results in Table 1) but also along the [-110] direction. We observed no

Table 2 Normal mismatch, strain free lattice parameter of epilayer, lattice misfit, and in plane elastic strain parallel to the interface

Sample	Normal mismatch $\Delta a_{\rm q}^{\perp}/a_{\rm h} \ (\times 10^{-3})$	Strain free lattice parameter of epilayer $a_q^{\text{s.f.}}(\text{nm})$	Lattice misfit $(\Delta a/a)_{\rm o}$ $(\times 10^{-3})$	Elastic strain $\varepsilon (\times 10^{-3})$
1	2.34	0.5660	1.17	-1.11
2	1.75	0.5658	0.88	-0.85
3	0.95	0.5656	0.48	-0.46
4	0.94	0.5656	0.47	-0.46
5	-0.67	0.5651	-0.33	0.32
6	-1.57	0.4549	-0.79	0.76
7	-1.76	0.5648	-0.88	0.85
8	-1.93	0.5648	-0.96	0.92
9	-3.72	0.5642	-1.86	1.76

difference in the two directions, in agreement with the finding in ref. [22] that anisotropy of relaxation (i.e. orthorhombic nature) is observed only for substantially relaxed samples.

In Fig. 2, a_q^{\parallel} calculated from the parallel mismatch is plotted as a function of a_q^{\perp} calculated from the normal mismatch. The dotted lines represent the lattice parameters of the GaAs substrate for reference. The five samples to the left side of the GaAs line are in tension because a_q^{\perp} is smaller than a_q^{\parallel} . The other samples are in compression because a_q^{\perp} is larger than a_q^{\parallel} . It is clear from this figure that Δa_q^{\perp} (distance between the triangle and GaAs $^{\perp}$) is considerably smaller than Δa_q^{\perp} (distance between the triangle and GaAs $^{\perp}$ line) as a result of tetragonal distortion, and that the heterointerface between the InGaP epilayer and the GaAs substrate is coherent, as evidenced by the high tetragonality factor of the samples.

3.2. Substrate X-ray line broadening

It is generally accepted that after epitaxial growth, the X-ray full width at half maximum (FWHM) of the substrate becomes larger than that of bare substrate. A similar trend was observed in our experiments. Three major factors are thought to lead to the substrate line broadening [24]: (i) presence of structural defects; (ii) inhomogeneity of chemical composition; (iii) elastic curvature of Bragg planes. The first hypothesis is excluded in our samples, since the X-ray topographs revealed no structural defects at the interface as mentioned earlier. We have performed Auger electron spectroscopy, and have observed no evidence of interdiffusion between the epilayer and the substrate. Composition gradients are thus unimportant in our samples. It is therefore thought that the line broadening observed in the GaAs substrate is caused by the misfit

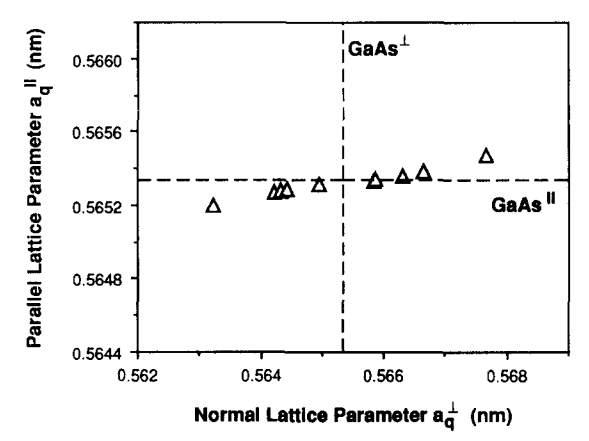


Fig. 2. Epilayer lattice parameter normal and parallel to the wafer surface, a_q^{\perp} and a_q^{\parallel} , respectively. The dotted lines show the GaAs lattice parameters for reference.

induced lattice curvature alone. Based on this, the substrate FWHM was measured and plotted as a function of the lattice misfit as shown in Fig. 3. The GaAs FWHM was measured from the (400) symmetric rocking curve using RADS (Rocking curve Analysis by Dynamic Simulation) program developed by Bede. Measurements were performed three times on three arbitrary points on the sample. Scatter was less than \pm 3%, showing good uniformity of the crystal across the sample. It can be seen from the figure that the lower FWHM, in general, is obtained for samples with the smaller lattice misfit. This dependence of the GaAs FWHM on the lattice misfit is attributed to the wafer curvature observed as described in the next section.

3.3. Misfit stress induced lattice curvature

If the lattice mismatched layers are bonded together, the wafer generally assumes an overall lattice curvature as a result of misfit stress [20,25]. Among various methods, the X-ray technique is very sensitive to small orientation differences in the crystal lattice. Consequently, it can be used to quantitatively measure the lattice curvature. A technique for measuring the curvature has been reported [26] in which the radius of curvature is directly calculated from the distance between diffraction lines recorded on a photographic film. However, due to the difficulty in precisely measuring the separation between diffraction lines, the automatic Bragg angle control technique was chosen as an alternative. A full description of this method is given elsewhere [27]. Briefly, if some part of the sample is brought into the reflecting position, other regions will not diffract properly, if the crystal is bent. Thus, the diffracted intensity will be lower, unless the specimen is rotated to restore the proper diffracting conditions. Hence, one can determine the radius of curvature by

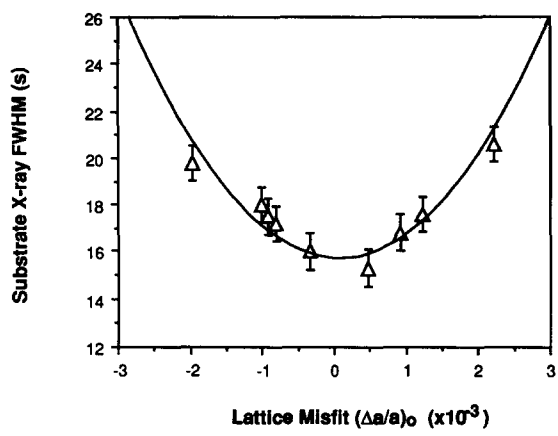


Fig. 3. Substrate X-ray FWHM plotted as a function of lattice misfit. A continuous line is drawn from the data points.

monitoring how much the crystal is rotated to bring it back into the reflecting position as one translates the specimen past the incident beam. The radius of curvature, R, is defined by

$$R = s/\delta \tag{8}$$

where s is the distance travelled on the specimen and δ is the amount of angular rotation to bring the specimen back into the diffracting condition. In all our samples, lattice planes are found to be deformed to spherical shape within experimental error.

Radii of curvature of all the samples were measured using this technique and plotted as a function of the lattice misfit as shown in Fig. 4(a). R ranges from 10 to 55 m depending on the degree of misfit. The larger R is obtained for the samples with the smaller lattice misfit. Note that R goes to infinity when the misfit approaches zero. In Fig. 4(b), R is plotted as a function of the elastic strain. It is evident from the figure that R is also dependent on the degree of elastic strain. R decreases with an increase in elastic strain in a non-linear fashion. It initially decreases substantially with a small increase in strain, and subsequently decreases to a lesser extent.

It is worthwhile to check the consistency of the measured R using the misfit stress model. R can be calculated by [20]

$$\frac{1}{R} = \frac{6t_{1}}{t_{0}^{2}} \frac{1}{1 + 6(t_{1}/t_{0})} \frac{1 - \nu}{1 + \nu} \times \left[\left(\frac{\Delta a_{q}^{\perp}}{a_{b}} \right) - \left(\frac{\Delta a_{q}^{\parallel}}{a_{b}} \right) \right]$$
(9)

where t_1 and t_0 correspond to epilayer and substrate thickness, respectively. The calculated R using this equation is compared with the measured value in Fig. 5. The theoretical data are seen to agree fairly well with

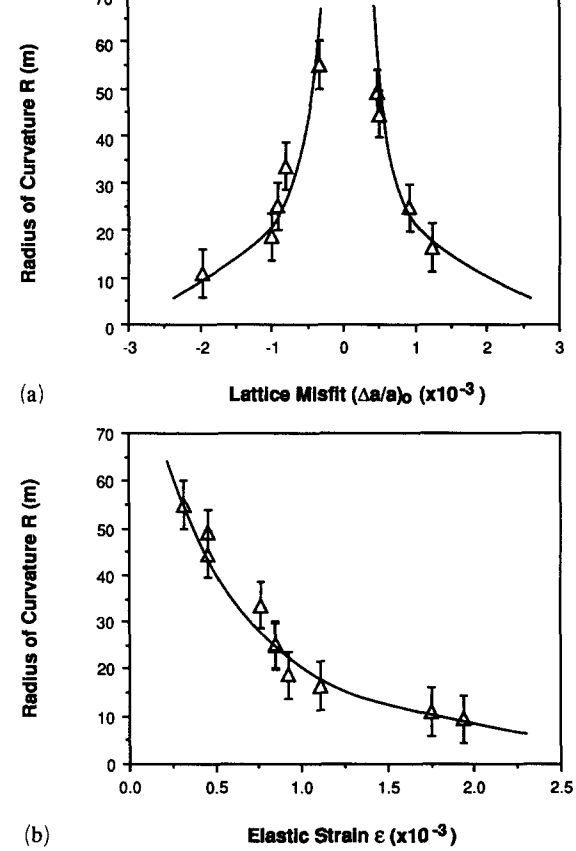


Fig. 4.(a) Radius of curvature, R, plotted as a function of lattice misfit. Larger R is obtained for the sample with smaller lattice misfit. (b) R plotted as a function of elastic strain.

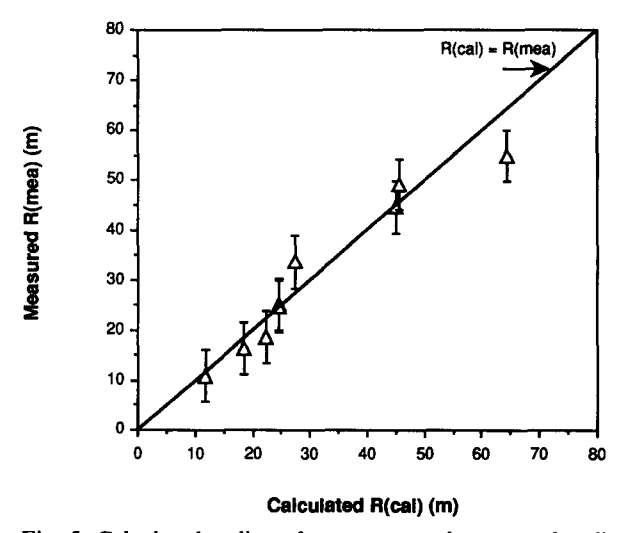


Fig. 5. Calculated radius of curvature and measured radius of curvature.

the experimental data. One important point to note from Eq. (9) is that when the parallel mismatch is comparable with the normal mismatch (as in the case of substantially relaxed specimen), the bent lattice relaxes

back to a flatter shape $(\Delta a_{\rm q}^{\parallel}/a_{\rm b} \rightarrow \Delta a_{\rm q}^{\perp}/a_{\rm b}, R \rightarrow \infty)$. This means that samples containing dislocations would have relatively large R even when they had large lattice misfit. No such trend is observed in our case as shown in Fig. 4(a), indicating the coherent nature of our samples.

3.4. Determination of misfit stresses

One of the important problems in the layered heterostructures is the presence of misfit stress introduced by lattice mismatch. Stress in the heterostructures depends not only on the mismatch, but also on the growth conditions such as growth temperature, growth rate, and the thickness of film and substrate. Thus, precise determination of the stress is essential to improve growth conditions and wafer quality [28]. If the radius of curvature of the sample is known, the stress can readily be estimated. This can be achieved using the following equation [20,28,29]

$$\sigma_{\rm R} = \frac{E}{6(1-\nu)} \frac{t_0^2}{t_1} \frac{1}{R} \tag{10}$$

where E is the elastic modulus. In this equation, $\sigma_{\rm R}$ represents the stress calculated from the radius of curvature. In determining the misfit stress using this equation, $E/6(1-\nu)$ is assumed to be 3.166×10^{11} dyn cm⁻² [30]. t_1 and t_0 are 1 and 350 μ m, respectively. Eq. (10) can then be simplified for our samples:

$$\sigma_{\rm R} = (3.88 \times 10^{12})/R \,(\rm dyn \, cm^{-2})$$
 (11)

There is an independent way to determine the misfit stress of the heterostructures using the linear elasticity. In this analysis, the misfit stress in the lateral direction, σ_{ϵ} , can be calculated assuming plane stress conditions $(\sigma_{xx} = \sigma_{yy}, \sigma_{zz} = 0)$:

$$\sigma_{c} = \{ E/(1-\nu) \} \varepsilon \tag{12}$$

Using the known values of ε (see Table 2), σ_{ε} can be easily calculated. In Eq. (12), σ_{ε} represents the stress calculated from the elastic strain. The misfit stresses in our samples calculated by Eqs. (11) and (12) are compared in Fig. 6. As can be seen, the misfit stress ranges from 8×10^8 to 4×10^9 dyn cm⁻² depending on the lattice misfit.

3.5. Curvature induced substrate line broadening

Once the radius of curvature is determined, it is a relatively simple matter to calculate the X-ray line broadening. It is well known that lattice curvature leads to line broadening [25]. This would be expected to arise from interaction of the misfit induced curvature with the finite width of the parallel X-ray beam. The

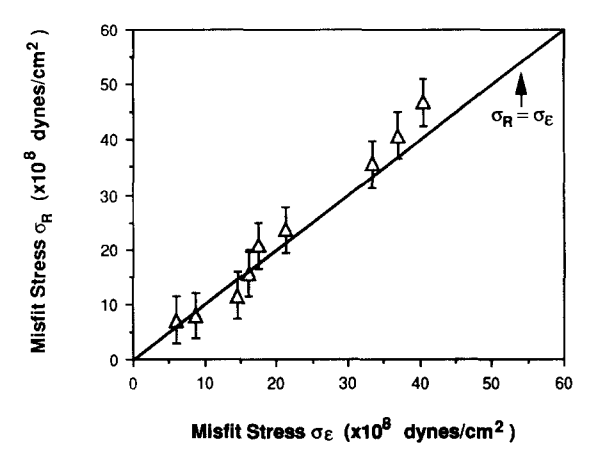


Fig. 6. Comparison of misfit stress σ_R calculated from the radius of curvature and σ_ϵ from linear elasticity.

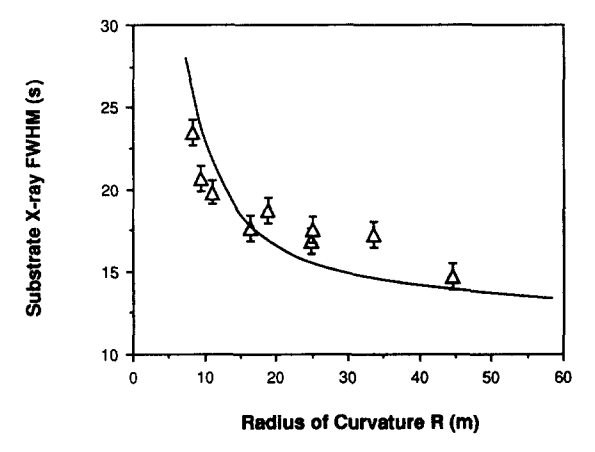


Fig. 7. Effect of radius of curvature on X-ray line width of substrate. A continuous line represents the calculated contribution to the X-ray line broadening.

X-ray line broadening caused by lattice curvature alone, β_R , is calculated using [9,31]

$$\beta_{\rm R}^2 = (W^2/R^2 \sin^2 \theta) \tag{13}$$

where β_R is the curvature contribution to the X-ray line width, W is the X-ray beam width (0.5 mm in our case), and θ is the Bragg angle. This calculation is shown as a continuous line in Fig. 7. In this figure, X-ray line widths of the substrate are correlated with the lattice curvature. The intrinsic components such as natural broadening determined by structure factor and the instrumental broadening are also incorporated into the calculation as a common factor such that the continuous line is a function of the curvature induced broadening only. Based on this, it can be shown that the continuous line in Fig. 7 is a function of curvature induced broadening alone as mentioned above. Good correlation between the measured and the calculated line width of the substrate demonstrates that the sub-

strate line broadening in the elastic range is determined essentially by the lattice curvature induced by the elastic strain.

3.6. Model for X-ray line broadening of substrate

Assuming a Gaussian shape of the X-ray rocking curve and a Gaussian distribution of the intensity of the rocking curve components [31], it may be assumed, especially for the substrate of single crystal heterostructures, that the X-ray line width consists of intrinsic broadening such as the natural line broadening and instrumental broadening, and misfit strain induced curvature:

$$\beta_{\rm C} = (\beta_{\rm N}^2 + \beta_{\rm I}^2 + \beta_{\rm R}^2)^{1/2} \tag{14}$$

where β_C is the total calculated line width, β_N is the natural line width of GaAs (9 s) [12], β_I is the instrumental broadening which can be determined by examining the X-ray spectrum of a high quality crystal whose half-width is known. β_R is the broadening due to curvature as mentioned above. The radius of curvature can also be determined by a misfit stress model [20]

$$\frac{1}{R} = \frac{6t_1}{t_o^2} \frac{1}{1 + 6(t_1/t_o)} \left(\frac{\Delta a}{a}\right)_o \tag{15}$$

From Eqs. (13) and (15), the theoretical value of β_R can be calculated by

$$\beta_{R} = \left[\left(\frac{6t_{1}}{t_{o}^{2}} \right) \frac{1}{1 + 6(t_{1}/t_{0})} (\Delta a/a)_{o} \right] \times \frac{W}{\sin \theta}$$
(16)

Combining Eq. (16) with Eq. (14), the estimate of the total rocking curve half width of the substrate of layered heterostructures can be obtained:

$$\beta_{\rm C} = \sqrt{\beta_{\rm N}^2 + \beta_{\rm I}^2 + \left[\left(\frac{6t_{\rm I}}{t_{\rm o}^2} \right) \frac{1}{1 + 6(t_{\rm I}/t_{\rm o})} \left(\frac{\Delta a}{a} \right)_{\rm o} \right]^2 \frac{W^2}{\sin^2 \theta}}$$
(17)

A critical comparison is made between the calculated line width, $\beta_{\rm C}$, and the measured line width, $\beta_{\rm M}$. This is summarized in Table 3. Some deviation of the measured FWHM from the calculated FWHM can be seen in the figure. This may be due to the presence of impurities and low density dislocations which are not detectable with X-ray topography. It is known [20] that the interfacial defects such as dislocations relax the wafer curvature, which in turn lead to variation of the broadening mechanism. Nevertheless, good agreement

Table 3
Components for substrate FWHM, and calculated and measured FWHM of substrate

Sample	$oldsymbol{eta_{N}}$	$oldsymbol{eta_1}$	$oldsymbol{eta}_{ extsf{R}}$	$oldsymbol{eta}_{ ext{C}}$	$oldsymbol{eta_{M}}$
1	9	8.8	11.1	15.8	17.6
2	9	8.8	8.3	15.1	16.8
3	9	8.8	4.5	13.4	14.7
4	9	8.8	4.4	13.3	15.3
5	9	8.8	3.1	12.9	16
6	9	8.8	7.4	14.6	17.2
7	9	8.8	8.4	15.1	17.5
8	9	8.8	9.1	15.5	18.7
9	9	8.8	17.9	21.8	19.8

 $\beta_{\rm R}$, curvature induced broadening; $\beta_{\rm I}$, instrumental broadening; $\beta_{\rm N}$, natural broadening of GaAs substrate; $\beta_{\rm C}$, calculated FWHM; $\beta_{\rm M}$, measured FWHM.

between the measured and the calculated values demonstrates that the major contribution to X-ray line broadening of strained substrate is stress-induced lattice curvature.

4. Concluding remarks

InGaP/GaAs, single heterostructure wafers are grown by MOCVD, and their interfacial coherency effects on the substrate line broadening are examined by DXRD. Lattice mismatches in both growth and parallel directions are determined. Elastic strain and strain-free lattice misfit are also calculated. Dependence of the substrate X-ray FWHM on lattice coherency is observed, and it is found that the lower FWHM is obtained for the sample with the smaller lattice misfit. This dependence is attributed to misfit stress induced lattice curvature, and the radius of curvature of the wafer is determined by the automatic Bragg angle control technique. The radius of curvature varies with the lattice misfit and the elastic strain, indicating that lattice curvature is responsible for the substrate line broadening. Misfit stresses calculated from curvature measurements are compared with those from linear elasticity. The substrate line broadening due to lattice curvature is calculated and is in good agreement with the measured value. Therefore, it is concluded that the major parameter influencing the line width of the substrate is strain-induced lattice curvature.

References

- [1] M. Ikeda, Appl. Phys. Lett., 51 (1987) 1572.
- [2] D.P. Bour and J.R. Shealy, Appl. Phys. Lett., 51 (1987) 1658

- [3] A.A. Rao, E.J. Caine, H. Kroemer, S.I. Long and D.I. Babic, J. Appl. Phys., 61 (1987) 643.
- [4] R.L. Hartman and A.R. Hartman, Appl. Phys. Lett., 23 (1973) 147.
- [5] G.H. Olsen and M. Ettenberg, J. Appl. Phys., 48 (1977) 2543.
- [6] A. Salokatve and M. Hovinen, J. Appl. Phys., 67 (1990) 3378.
- [7] C.R. Wie, J. Appl. Phys., 65 (1989) 2267.
- [8] R.J. Baird, H. Holloway, M.A. Tamor, M.D. Hurley and W.C. Vassell, J. Appl. Phys., 69 (1991) 226.
- [9] S.B. Qadri and J.H. Dinan, Appl. Phys. Lett., 47 (1985) 1066.
- [10] P. Gay, P.B. Hirsch and A. Kelly, Acta Metall., 1 (1953) 315.
- [11] M.A.G. Halliwell, M.H. Lyons, B.K. Tanner and P. Ilczyszyn, J. Cryst. Growth, 65 (1983) 672.
- [12] C. Ferrari and P. Franzosi, J. Appl. Phys., 65 (1989) 1544.
- [13] J. Matsui, K. Onabe, T. Kamejima and I. Hayashi, J. Electrochem. Soc., 126 (1979) 664.
- [14] K. Oe, Y. Shinoda and K. Sugiyama, Appl. Phys. Lett., 33 (1978) 962.
- [15] D.K. Schroder, Semiconductor Material and Device Characterization, New York, 1990.
- [16] S. Weissmann, Application of X-Ray Topographic Methods to Materials Science, Plenum, New York, 1984.
- [17] G.A. Rozgonyi and D.C. Miller, *Thin Solid Films*, *31* (1976) 185
- [18] J. Chaudhuri, S. Shah and J.P. Harbison, J. Appl. Phys., 66 (1989) 5373.

- [19] G.H. Olsen, C.J. Nuese and R.T. Smith, J. Appl. Phys., 49 (1978) 5523.
- [20] S.N.G. Chu, A.T. Macrander, K.E. Strege and W.D.J. Johnston, J. Appl. Phys., 57 (1985) 249.
- [21] V. Swaminathan and A.T. Macrander, Materials Aspects of GaAs and InP Based Structures, Prentice Hall Reference Series, Prentice Hall, Englewood Cliffs, NJ, 1991.
- [22] B.R. Bennett and J.A.D. Alamo, J. Electron. Mater., 20 (1991) 1075.
- [23] B.R. Bennett and J.A.D. Alamo, J. Appl. Phys., 73 (1993) 3195.
- [24] C. Bocchi, C. Ferrari and P. Franzosi, J. Electron. Mater., 16 (1987) 245.
- [25] M.A.G. Halliwell, M.H. Lyons and M.J. Hill, J. Crystal Growth, 68 (1984) 523.
- [26] C.L. Kuo, Y.H. Kao, E. Arnold and J.C. Bilello, J. Appl. Phys., 64 (1988) 1791.
- [27] G.A. Rozgonyi and T.J. Ciesielka, Rev. Sci. Instrum., 44 (1973) 1053.
- [28] C. Li, Z. Mai, S. Cui, J. Zhou and A. Ding, J. Appl. Phys., 66 (1989) 4767.
- [29] A. Brenner and S. Senderhoff, J. Res. Natl. Bur. Stand., 42 (1949) 105.
- [30] K. Lal, S. Niranjana and N. Goswami, J. Appl. Phys., 67 (1990) 4105.
- [31] M.J. Hordon and B.L. Averbach, *Acta Metall.*, 9 (1961)
- [32] K. Sugii, H. Koizumi and E. Kubota, *J. Electron. Mater.*, 12 (1983) 701.